Non-destructive evaluation of ammonium oxalate treatment penetration depth using micro-SORS

A.Botteon[a,b*], C.Castiglioni[b], P.Matousek[c,] M.Realini[a] , C.Colombo[a], and C.Conti[a*]

[a] Consiglio Nazionale delle Ricerche, Istituto di Scienze del Patrimonio Culturale (ISPC), Via Cozzi 53, 20125, Milano, Italy.

[b] Politecnico di Milano, Department of Chemistry, Materials and Chemical Engineering "G. Natta", piazza Leonardo da Vinci 32, 20131 Milano, Italy.

[c] Central Laser Facility, Research Complex at Harwell, STFC Rutherford Appleton Laboratory, UK Research and Innovation (UKRI), Harwell Oxford, OX11 0QX, United Kingdom.

* Corresponding authors: alessandra.botteon@cnr.it, claudia.conti@cnr.it

Abstract

The determination of the penetration depth of treatments is a crucial issue in conservation science for assessing the treatments efficacy. Micro-spatially offset Raman spectroscopy (micro-SORS), that permits the non-destructive collection of Raman photons generated under the surface of a turbid material, here has been used to non-destructively retrieve the distribution of oxalates formed after ammonium oxalate (AmOX) treatment inside plasters. Two sets of samples treated with AmOX have been studied, plaster mock-ups and plaster fragments collected from the painted façades of Palazzo Besta in Teglio (Sondrio, Italy). The evaluation of the distribution of the newly formed oxalates was carried out considering the slope of the oxalates/calcite Raman bands intensity decay trend with increasing micro-SORS defocusing distance. Micro-SORS outcomes were found to be consistent with those obtained with conventional micro-Raman performed on cross-section, confirming the extension of this innovative method to the evaluation of treatments efficacy.

Keywords: micro-Spatially Offset Raman Spectroscopy, inorganic treatment, ammonium oxalate, calcium oxalate, penetration depth, non-destructive, Cultural Heritage

Graphical abstract
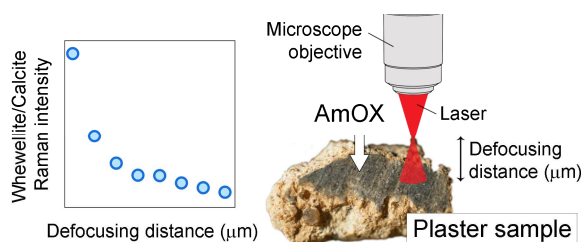
1. Introduction

Carbonatic materials as limestones, marbles and plasters have been extensively used in sculptures, monuments and buildings of cultural interest from ancient times to present days. Carbonatic materials are prone to weathering, due to the solubilization of carbonates, predominantly as a consequence of interaction with atmospheric water (rain and humidity), especially in acidic conditions [1].

To restore carbonatic weathered stones and plasters, and to prevent their further degradation, several products can be used, both organic and inorganic.

The use of inorganic-mineral treatments, over the last decades, has progressively increased because of their durability and higher compatibility with common substrates compared with organic compounds [2-3]. Among inorganic-mineral treatments, ammonium oxalate (AmOX, $(NH_4)_2C_2O_4$) and di-ammonium phosphate (DAP, $(NH_4)_2HPO_4$) are currently in the spotlight of scientific research on this topic [4-9], showing satisfying performance on several carbonatic substrates. These products undergo a reaction with the carbonatic matrix, and the lower solubility of newly formed crystalline phases assures a better decay resistance of the matrix.

The evaluation of the effectiveness of a treatment is crucial in conservation science for better assessment and planning of conservation actions, and the penetration depth of the treatment can be considered a key parameter in assessing its performance [10]. The depth reached by a treatment primarily depends on the type of product and the application methodology (such as product amount and concentration of applied solutions, use poultice or brush to spread the product and poultice contact time) as well as the substrate characteristics (such as porosity and pore size distribution in stones, aggregate type and aggregate size distribution in plasters) [11-12]. Given the number of parameters that influence the treatment penetration depth, its prediction *a priori* is extremely challenging. To date, the most promising approach for the study of penetration depth consists on the use of analytical techniques able to track the product inside the matrix after its application. Among the analytical methods, non-invasive and non-destructive ones are naturally preferred when dealing with Cultural Heritage material as they permit *in-situ* analysis or, in case of sampling, the fragments do not need any preparation (in contrast with cross-sections) and remain intact after the analysis.

Here, for the first time, the feasibility of using a non-destructive analytical method, namely micro-spatialy offset Raman spectroscopy (micro-SORS) [13-14], with high chemical selectivity and easy access is explored for the study of treated plasters, with high impact in conservation field. The technique was used here for the investigation of carbonatic plasters treated with AmOX, to track the distribution of newly formed oxalate phases.

Typically, AmOX treatment consists in putting in contact a water solution of this compound with the surface (*e.g.* poultice or application with a brush). AmOX is absorbed by the substrate, and its reaction with calcium carbonate leads to the formation of calcium oxalate, that is able to restore the stone or plaster network. Usually, whewellite, the monohydrate form of calcium oxalate ($CaC_2O_4 \cdot H_2O$) is predominantly formed; weddellite, the di-hydrate, metastable phase ($CaC_2O_4 \cdot 2H_2O$) converts to whewellite under certain conditions. Nonetheless, on historical buildings, monuments and artifacts, weddellite has been detected as both decay product and as a result of a treatment [15-18].

Moreover, if magnesium-containing carbonates are present (*e.g.* dolomite, magnesite or Mg-calcite), their reaction with AmOX lead to the formation of glushinskite ($MgC_2O_4 \cdot 2H_2O$) [19].

The application of AmOX treatment in several conservation sites over the last years demonstrated the protective role of calcium oxalate. In fact, its lower solubility in both neutral and acid pH environments compared to calcium carbonate prevents surface corrosion [20-21]. The moderate increase of colour saturation of the surface is a further treatment effect, probably related to the reduction of the surface micro-roughness [21].

To date, the study on the penetration depth of oxalates in carbonatic matrices has been carried out with both destructive and non-destructive approaches. Destructive methods involved the analysis of cross-sections with conventional micro-Raman mapping [4, 17, 22-23], ATR μ-FTIR [3], as well as measurements with sincrotron radiation micro X-ray powder diffraction (SR-μ-XRPD) [20]. Non-destructive methods also include neutron tomography on carbonatic stones [24-25], but this technique lacks chemical selectivity and accessibility.

Here, micro-SORS is used for the analysis of two sets of plaster samples: the first set is made of mock-up plasters treated with AmOX; the second set consists in plaster fragments collected from the painted façades of the internal court of Palazzo Besta in Teglio (Sondrio, Italy) after AmOX treatment. Defocusing [26], the most basic variant of micro-SORS, was used; in this variant, the Raman signal of the sample inner portions is preferentially collected by enlarging the laser and the collections areas on the sample surface. This enlargement is achieved with a simple motion of the sample in z direction, typically away from the in-focus position. To date, micro-SORS has been predominantly used to retrieve the composition of micro-layered, turbid systems, and recently the possibility of using this technique to non-destructively study the diffusion of an agent in a turbid matrix was explored [27-29]. Up to now, the diffusion was studied in largely homogenous systems; here the study is extended to more complex materials, which constitute a new challenge for micro-SORS due to their morphological and compositional heterogeneity. The degree of complexity increases with samples of historical plasters, as they often include additional decay products and conservation treatments previously applied.

The distribution of the newly formed calcium oxalate, here, was evaluated by considering the slope of the agent/matrix Raman intensity ratio trend, that was previously found to correlate with the penetration depth of the agent into matrix [29].

2. *Research Aim*

This research aims at exploring micro-SORS capability of obtaining non-destructive information about AmOX treatment distribution inside mock-ups plasters and plaster fragments collected from a historical building. The measurements here presented were carried out to prove that micro-SORS can differentiate the samples basing on the penetration depth of the treatment.

3. *Materials and Methods*

3.1 Plaster samples

The mock-up plaster samples (OX13, OX15 and OX23) were prepared using a lime binder and carbonatic aggregate (calcite and dolomite, grain size ranging from 80 μm to 500 μm). The mock-ups (5x5 cm) exhibit a 3 mm thick plaster layer applied on a carbonatic stone substrate. A yellow ochre paint was applied on the plaster surface with "a fresco" technique. After complete carbonation (4 months in a wet box with a carbon dioxide enriched atmosphere), the plasters were treated by placing on the specimens surface a cellulose poultice soaked with approximately 18 ml of 5% AmOX water solution. The poultice was kept in contact for 5 hours, refilling the solution every hour. For OX13 and OX15, a total of 4.8 ml of AmOX solution was

refilled on the poultice, while a refill of 19.2 ml was added on OX23. These samples were built up and analysed in a previous study with conventional micro-Raman measurements in cross-sections to determine the distribution of the newly formed calcium oxalate inside the plaster matrix [23]. Here, due to fluorescence, the yellow paint on the surface was removed (about 25 μm).

Palazzo Besta painted plasters (PB50 and PB52, displayed in Figure 1a and 1b) has been collected after AmOX treatment with the aim of restoring the micro-structure of the carbonatic paint layer and the plaster immediately underneath it. In the figure are also shown the building (Figure 1c) and the painted façades of the internal court, with indication of the sampling area (Figure 1d). As described in the previous set of samples, the treatment was carried out by placing the plaster in contact with a poultice soaked with 5% of AmOX in water solution for 5 hours. Sample PB50 was collected from an area that was treated only once, whereas in PB52 the treatment was applied twice.

Figure 1. PB50 (a) and PB52 (b) fragments used in micro-SORS measurements; Palazzo Besta (c) and detail of the painted façades of the internal court with indication of the sampling area (white square) (d).

The cross-sections for conventional Raman analysis were obtained by embedding the sections in epoxy resin and then cutting and polishing the exposed surface. Table 1 gives the summary of sample characteristics.

Table 1. Summary of the characteristics of the samples.

	Origin	AmOX water solution (C % w/w)	Contact time (h)	Other information	Oxalates penetration depth
OX13	Mock-up	5	5	Addition of 4.8 ml of AmOX water solution	135 µm*
OX15	Mock-up	5	5	Addition of 4.8 ml of AmOX water solution	135µm*
OX23	Mock-up	5	5	Addition of 19.2 ml of AmOX water solution	425 µm*
PB50	Palazzo Besta	5	5	-	390 µm**
PB52	Palazzo Besta	5	5	two treatment applications	450 µm**

* Determined with conventional micro-Raman measurement on cross-sectioned samples, see [23].

** Determined with conventional micro-Raman measurement on cross-sectioned samples in this study.

3.2 Conventional micro-Raman measurements on cross-sections and micro-SORS measurements

All the Raman measurements were collected using a Senterra dispersive Raman microscope (Bruker Optik GmbH) equipped with a Peltier cooled charge coupled device (CCD) detector (1,024 × 256 pixels), a 785 nm excitation laser and a 400 grooves/mm grating. 10 micrometre-step SORS series were collected on different locations on the surface of the samples using a 20x microscope objective and a 50x1000 µm slit.

The measurements on cross-sections of samples PB50 and PB52 were collected in mapping modality, using a 50x microscope objective and a 50µm pinhole. The spectra were collected using 10 mW laser power, and an acquisition time of 25s (5s and 5 co-additions). The step size of the maps was approximately 50 µm in both the x and y directions. The maps covered, in total, an area of approximately 2.5 mm in x direction, and 500-800 µm in y direction on each sample.

The maps were baseline corrected and maximum-minimum normalized to the 1240-400 spectral region. Oxalates distribution was obtained by integrating the Raman bands included in the 1505-1446 region of the spectra (the 1475 cm^{-1} band of weddellite, the 1471 cm^{-1} band of glushinskite, the 1462 and 1488 cm^{-1} bands of whewellite). The maps obtained from different areas of the samples were merged, and the colour scale of the integrated bands was set to the same limits, to facilitate the visual comparison of calcium oxalate distribution in the mapped areas. The penetration depth of calcium oxalate was estimated by monitoring the presence of Raman bands of calcium oxalate *y* line by *y* line in the maps. The maximum penetration depth of the treatment obtained by the *y* lines (48 lines in PB50 and 41 lines in PB52) was then averaged to obtain a representative calcium oxalate penetration depth in the two samples.

With regards to micro-SORS measurements, on the mock-ups (OX13, OX15, OX23), the spectra were collected at imaged position and at up to 1500 μm defocusing distances, with z step size of 100 μm. A laser power of 50 mW and an acquisition time of 100s (10s and 10 co-additions) were used.

On the historical plaster samples (PB50 and PB52), the spectra were collected at imaged position and at 50, 100, 150, 200, 250, 300, 350, 400, 500, 600, 700 and 800 μm defocusing distances. In this set, the Raman spectra obtained with larger defocusing distances were too noisy for a reliable monitoring of Raman bands intensity, and smaller defocusing steps were used to maximize the information retrievable from the sample. A laser power of 100 mW and an acquisition time of 100s (10s and 10 co-additions) were used.

For the mock-ups, the micro-SORS spectra obtained at the same defocusing distances were averaged and the maximum height of selected whewellite and calcite Raman bands (1462 cm^{-1} and 1087 cm^{-1} respectively) were used to calculate the Raman intensity ratios to build a ratio plot.

For Palazzo Besta samples (PB50 and PB52) the ratios were calculated using a Raman band of an oxalate species (the 1462 cm^{-1} Raman band of whewellite, or the 1475 cm^{-1} Raman band of weddellite, or the 1471 cm^{-1} Raman band of glushinskite) and the 1087 cm^{-1} Raman band of calcite. The ratio values were also averaged to obtain representative ratio trends for the two samples.

Origin software (2021b) was used for micro-SORS Raman bands intensity calculation and plot construction; OPUS software for maps elaborations.

4. Results and Discussion

4.1 Conventional micro-Raman measurements on mock-up plaster cross-sections

The measurements performed on the mock-ups cross-sections [23] revealed that whewellite is present in all samples, while no weddellite was detected. Samples OX13 and OX15, treated in the same way, were found to possess the same penetration depth of the treatment (160 μm) whereas in OX23, treated with a more abundant refill of reagent, whewellite was detected up to 450 μm depth. Details about the product distribution inside the plasters can be found in the abovementioned publication [23].

Here, since the paint on the surface (about 25 μm) was removed, the whewellite penetration depth is of approximately 135 μm in OX13 and OX15, and 425 μm in OX23.

4.2 Micro-SORS measurements on mock-up plaster samples

On the surface of the samples, the characteristic Raman signatures of calcite and whewellite can be observed (calcite bands at 1087, 714, 278 and 152 cm^{-1}, whewellite bands at 1488, 1462, 895, 595, 520, 503, 195 and 140 cm^{-1}); moreover, the presence of dolomitic aggregate gives rise to a shoulder at 1097 cm^{-1} on the 1087 cm^{-1} band of calcite (Figure 2). The 380 cm^{-1} Raman band is attributed to a residue of the painted layer, made of yellow ochre (goethite). OX23 shows more intense Raman bands of whewellite compared to OX13 and OX15, suggesting that the more abundant AmOX refill used to treat OX23 plaster led to the formation of more calcium oxalate on the sample surface.
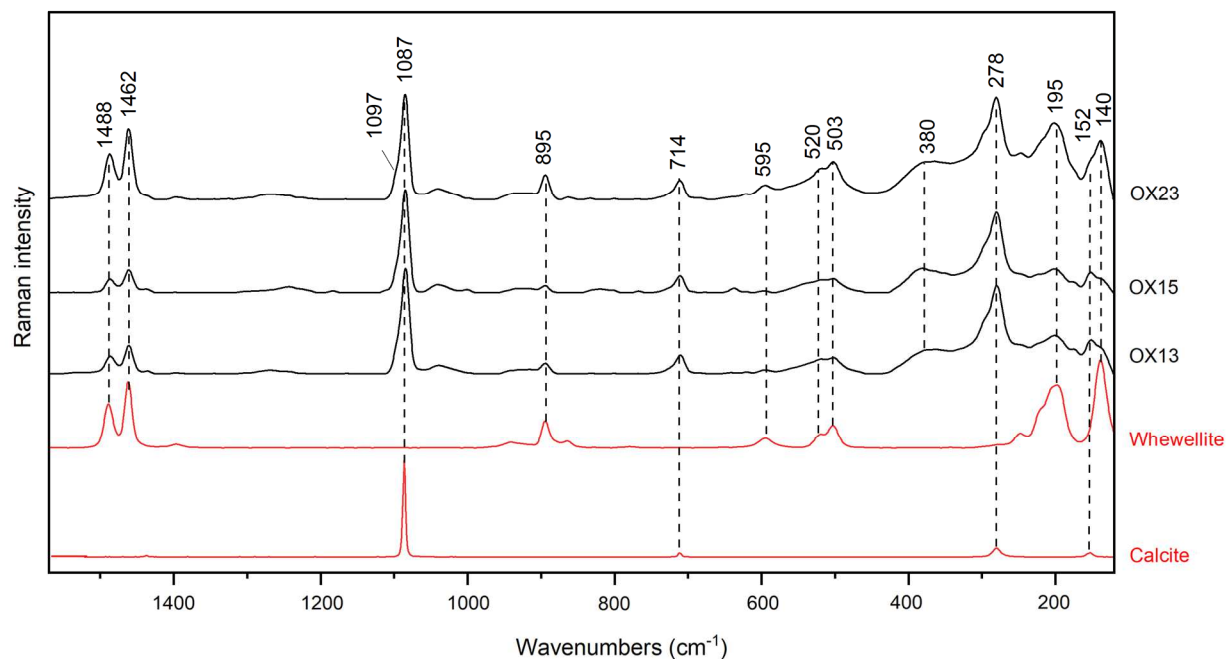
Figure 2. Raman spectra (imaged position) obtained on the surface of OX13, OX15 and OX23. Reference spectra of calcite and whewellite are shown.
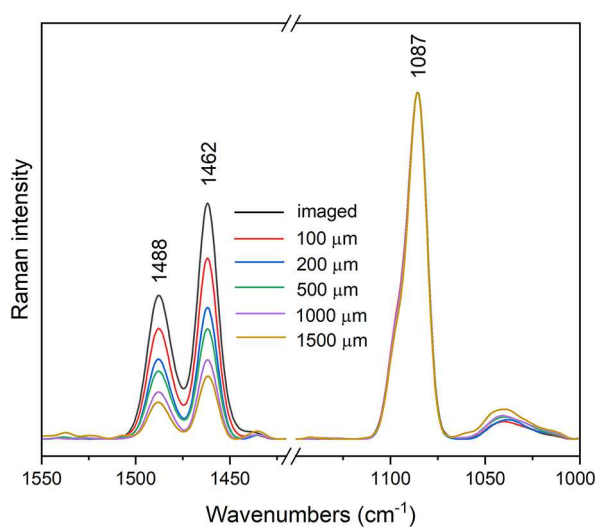

Figure 3. Average micro-SORS spectra collected on OX23. The imaged spectrum and the spectra at different defocusing distances are shown, normalized to calcite Raman band (1087 cm^{-1}). Whewellite Raman bands (1462 cm^{-1} and 1488 cm^{-1}) decrease with increasing defocusing distance.

The whewellite/calcite Raman intensity ratio of the three samples show a decreasing trend with the increase of the defocusing distance, as it is shown in Figure 3, where the average Raman spectra of sample OX23 are representatively shown. The spectra are normalized to the 1087 cm^{-1} Raman band of calcite to highlight the change of whewellite intensity. Whewellite Raman bands (1462 cm^{-1} and 1488 cm^{-1}) decrease with the increase of the defocusing distance, demonstrating a decrease of whewellite abundance with the increase of depth.

The whewellite/calcite Raman intensity ratio plot is shown in Figure 4a as a function of the defocusing distance. The decreasing trend observed for the three samples is related to the progressive decrease of whewellite in the inner portion of the plaster. OX13 and OX15, treated in the same way, produce very similar ratio trends, as expected, suggesting a similar diffusion of the treatment. Higher ratio values are obtained in OX23, according with the Raman spectra obtained on the samples' surface where a more abundant presence of whewellite is observed. To obtain information about the penetration depth of the product, a normalization is applied to ensure the accurate comparison among the samples (Figure 4b). The normalization is applied to the ratio value at 300 μm defocusing, to avoid the uncertainty of the ratios obtained at imaged position in line with a methodology adopted in a previous study to suppress sensitivity to local heterogeneity of material composition [29]. Moreover, as demonstrated in this earlier, the slope of the decay curve correlates directly with the agent penetration depth. Accordingly, the steeper decrease of the ratio values observed in OX13 and OX15 is related to the smaller penetration depth of whewellite in these two samples than in OX23.

The slope of the linear fit was used to build the slope plot in Figure 5, allowing to easily visualize and compare the samples.

OX13 and OX15 slopes are closer than that for OX23. Moreover, the confidence intervals of OX13 and OX15 are partially overlapped, indicating that a similar depth of whewellite is present in OX13 and OX15. The smaller slope (absolute) value of OX23 correlates with a higher penetration depth of whewellite. This outcome is consistent with the results of micro-destructive measurements performed in cross-section by Conti et al. [23].
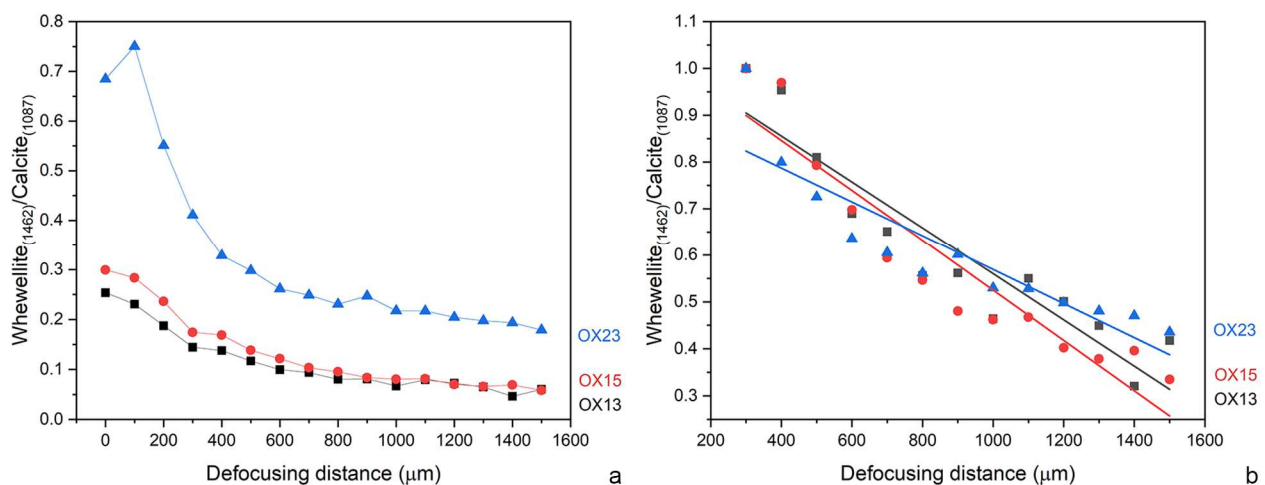

Figure 4. Not-normalized (a) and normalized (b) ratio plot of OX13, OX15 and OX23 with linear fitting.
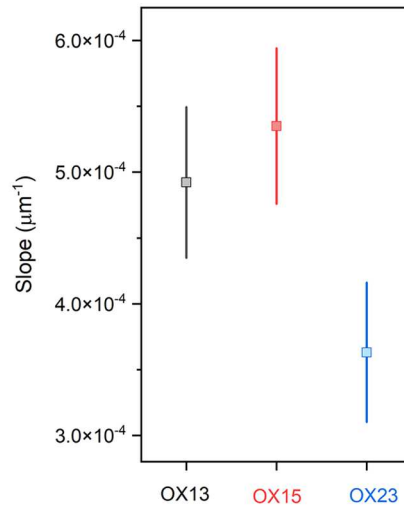
Figure 5. OX13, OX15 and OX23 slopes (absolute values) with confidence interval of the linear fitting derived from Fig 5b

<u>*4.3 Conventional micro-Raman measurements on historical plaster cross-sections*</u>

The Raman maps collected on cross-sections revealed the presence of calcite, whewellite, weddellite and glushinskite in the plaster binder. The integration of the Raman bands in the 1505-1446 cm^{-1} range allowed visualizing the distribution of the treatment inside the plasters (Figures 6a and b). The treatment is non-homogeneously distributed: in some areas, oxalates are more abundant on the surface than in the portion immediately underneath, whereas a reverse situation has been observed in other areas.

Oxalates Raman signals were detected up to 650 μm in PB50 and up to 700 μm in PB52, with an average penetration depth of 390 μm in PB50 (St. Dev = 141 μm) and 450 μm in PB52 (St. Dev = 179 μm).
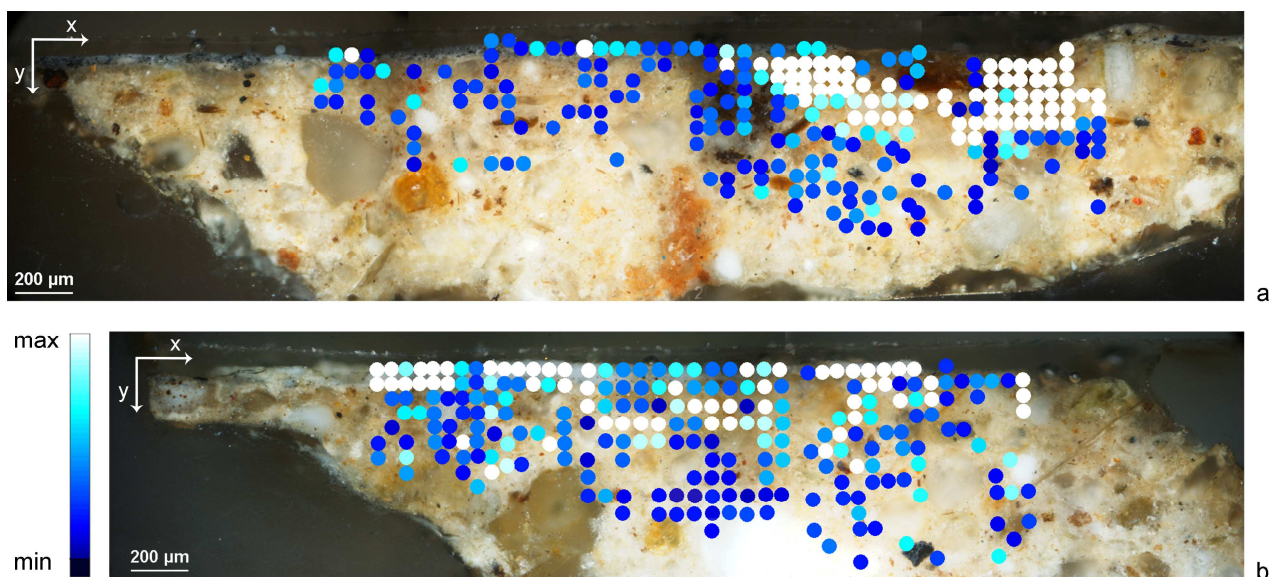

Figure 6. Cross-section of PB50 (a) and PB52 (b). The dots represent the distribution of oxalates and were obtained integrating the 1505-1446 cm^{-1} spectral region in the micro-Raman maps. The colour scale is displayed at the bottom left.

4.4 Micro-SORS measurements on historical plasters

The Raman spectra obtained on the samples surface revealed the presence of calcite, whewellite, weddellite, glushinskite and carbon black. The average of 10 spectra obtained on the surface of the two samples is reported in Figure 7. Carbon black (Raman band at 1325 cm^{-1}) is the pigment responsible for the grey colour of the painted area.

Whewellite (Raman bands at 1488, 1462, 895, 595, 503, 195 and 140 cm^{-1}) and weddellite (Raman bands at 1475, 910, 595, 503 and 190 cm^{-1}) are the reaction products of AmOX with calcite (Raman bands at 1087, 714, 278 and 152 cm^{-1}) that is a component of both paint layer and plaster matrix. Glushinskite (Raman bands at 1471, 913, 525 and 227 cm^{-1}) is the result of the reaction between AmOX and magnesium specie(s) of the binder (Mg-calcite).

The relative intensities of whewellite, weddellite and glushinskite were found to vary on the samples surface, revealing an uneven distribution of the phases (see Supplementary Material, Figure S1).

In line with expectations, the area treated with two AmOX treatments (PB52) was found to have higher oxalates Raman bands intensity compared to PB50, and this is related to a more abundant presence of oxalates on the surface of the material.
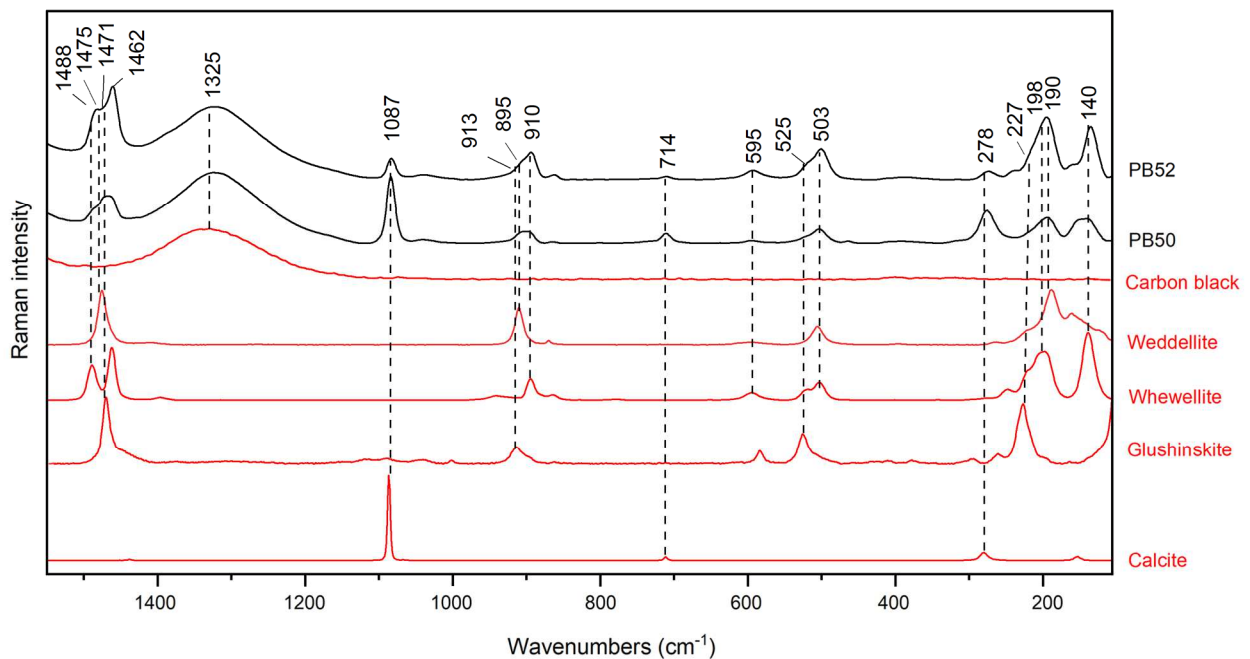

Figure 7. Average Raman spectra obtained on PB50 and PB52 surface. Reference spectra of calcite, whewellite, weddellite, glushinskite and carbon black are shown (red line).

Micro-SORS series collected on PB50 and on PB52 are representatively displayed in Figures 8a and 8b, respectively, normalized to calcite Raman band at 1087 cm^{-1}. Oxalate phases decrease compared to calcite, changing their relative intensities with increasing defocusing distance. This indicates a non-homogeneous distribution of the oxalate phases inside the plaster: PB50 imaged spectrum (Figure 8a) is dominated by glushinskite Raman band at 1471 cm^{-1} and, with the increase of the defocusing distance, whewellite and weddellite Raman bands emerge at 1462, 1475 and 1488 cm^{-1}. With regard to PB52 (Figure 8b), only whewellite is visible at imaged position and at 600 μm of defocusing distance, whereas both whewellite

(1462 and 1488 cm⁻¹) and weddellite (1475 cm⁻¹) are visible at 200, 400 and 800 µm of defocusing distances.

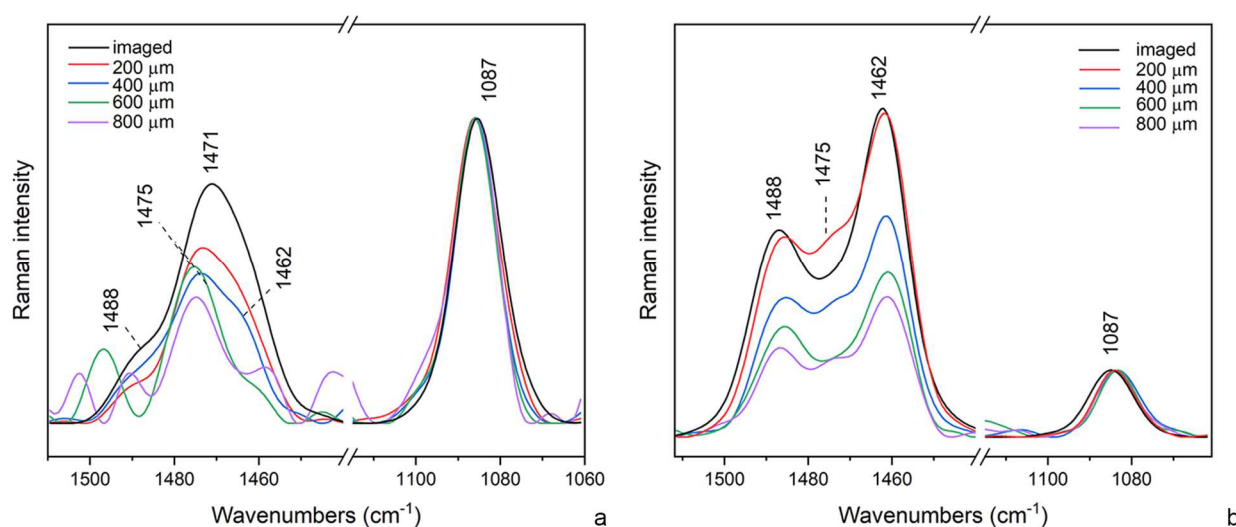Figure 8. Series of micro-SORS spectra acquired on PB50 (a) and PB52 (b). The spectra are normalized to 1087 cm⁻¹ Raman band of calcite. The oxalates (whewellite at 1462 and 1488 cm⁻¹, weddellite at 1475 cm⁻¹ and glushinskite at 1471 cm⁻¹) decrease their intensities with the increase of the defocusing distance.

For the ratio calculation, the maximum intensity of one of the Raman bands included in the range between the 1450 and 1500 cm⁻¹ is considered (the 1462 cm⁻¹ Raman band of whewellite, or the 1475 cm⁻¹ Raman band of weddellite, or the 1471 Raman band of glushinskite). In this way, information about the treatment penetration is obtained independently from the phases intensity fluctuations.

The single micro-SORS series obtained in PB50 and PB52 are reported in the ratio plot in Figure 9 a and b, respectively. Micro-SORS ratios revealed uneven trends: both increasing and decreasing trends are observed, and this outcome, that is consistent with cross-sectional measurements, is reasonably related to the extreme heterogeneity of the plaster composition, where the aggregate plays a major role in a non-uniform distribution of oxalates on both the surface and in the subsurface. The presence of a non-homogeneously distributed mixture of crystalline phases demonstrates that, unsurprisingly, a much more complex systems is generated when treating historical materials compared to *ad hoc* mock-ups. In fact, many variables which are quite common in historical plasters such as the presence of decay products, a heterogeneous composition of the aggregate and a largely heterogeneous aggregate particles size distribution, and the presence of holes and fractures, could increase the degree of the matrix heterogeneity, both chemical and morphological, resulting in a non-homogeneous treatment.

To obtain a representative ratio trend for the two samples, the single series were averaged. The averaged ratios are shown in Figure 9c, where it is clear that in PB52 the double treatment favoured the reaction with calcite, resulting in higher calcium oxalate/calcite Raman intensity ratios. For a better visualization of PB50 trend, the averaged ratios are singularly shown in Figure 9d.

In the average trend for both the samples, the ratio values decrease with the increase of the defocusing distance, and this is related to the overall decrease of oxalates with depth. Similarly to the previous set of samples, the ratios were normalized to make the trends comparable (Figure 9e). The plot shows a certain degree of fluctuation of the ratio values, that is related to the large variability of the trends of individual

series. A linear fitting was applied to the normalized ratio values, and the slope of the linear fit was used to build the slope plot in Figure 9f.
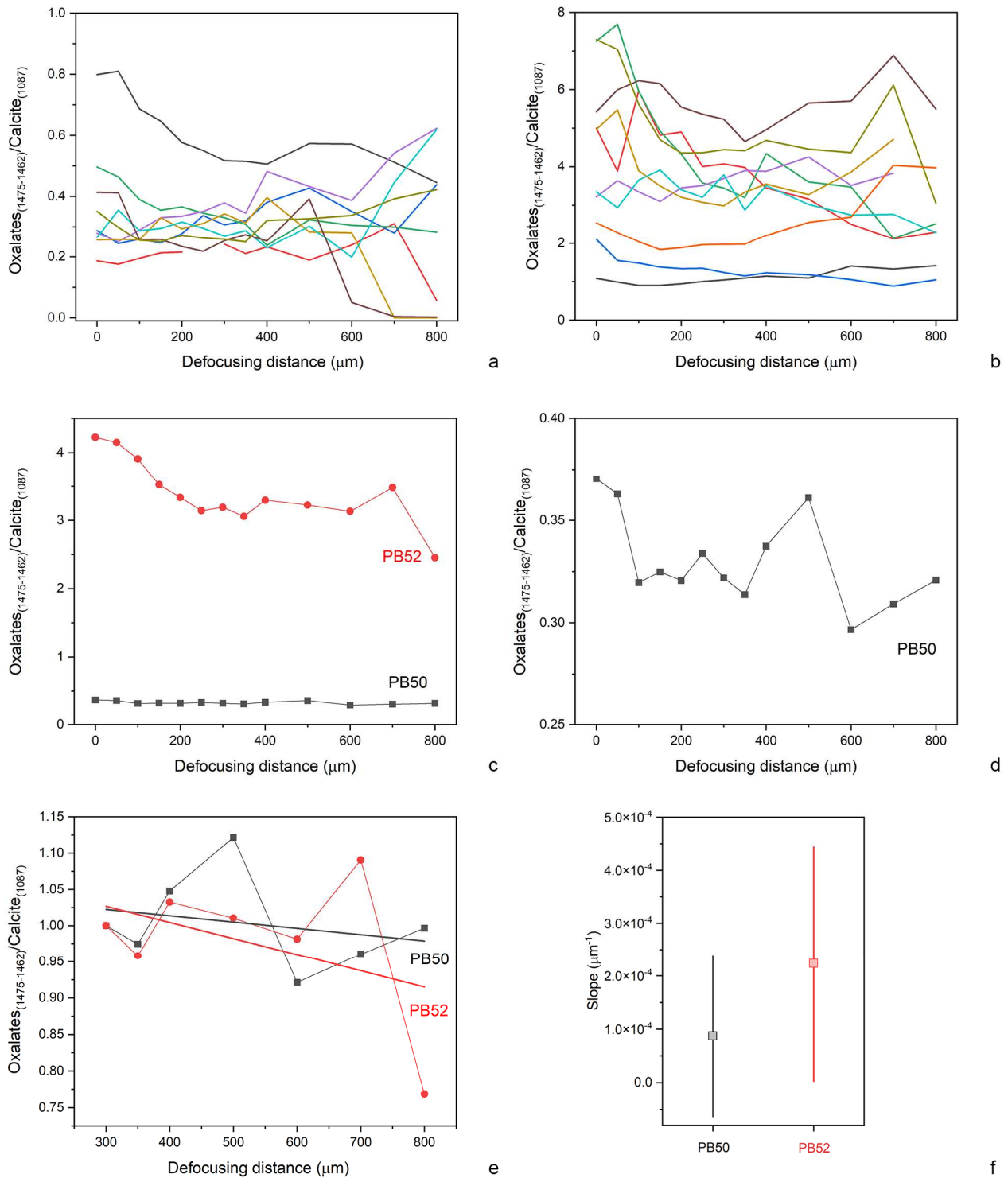
Figure 9. Ratio trends of the single series of PB50 (a) and PB52 (b); average ratio trend of PB50 and PB52 (c); PB50 average ratio trend with re-scaled y values (d); normalized ratio trend with linear fitting of samples (e); slope plots of PB50 and PB52 (f).

Pb50 shows a rather flat trend, according to the confidence interval of its slope that includes both positive and negative values. This outcome suggests a low degree of change of oxalates and calcite between the

surface and the subsurface. In other words, oxalates are not abundant on the sample surface, but the persistence of their Raman signal also at large defocusing distances suggests their presence also at a relatively large depth inside the material.

PB50 and PB52 confidence intervals are largely overlapped, suggesting that similar penetration depth of the treatment is obtained in the two samples, confirming the scenario achieved with conventional Raman maps on cross-sections. Micro-SORS does not appear to be sensitive to the small difference of the penetration depth values obtained in cross sections. It is also worth noting that Raman maps were performed on different fragments compared to the areas analysed with micro-SORS and in case of heterogeneous systems this could lead to slightly different penetration depths.

5. *Conclusions*

Here it is demonstrated that defocusing micro-SORS can be used to non-destructively study the penetration depth of AmOX treatments, also in complex and heterogenous systems as historical plasters. Micro-SORS results obtained on the two sets of plaster samples are consistent with those achieved with micro-Raman measurements on cross-sections, demonstrating micro-SORS reliability. This study paves way for the use of micro-SORS as a routine method for non-destructively evaluating the distribution of conservation products and addressing the choice towards more effective treatment procedures. In future, these studies could be extended to *in-situ* measurements using portable micro-SORS devices. In this way, the monitoring of the product inside the plaster could be derived through the analysis of a larger number of areas, which is critically important with heterogeneous systems.

At this stage, micro-SORS measurements do not determine absolute depth penetration of the treatment, instead they establish if the treatment is more or is less deeply penetrated in a sample compared to another sample. To provide absolute values of penetration depth a calibration of the system is needed, that implies a destructive study of plaster fragments with different penetration depth of the products.

Micro-SORS limits of detection (sensitivity) can be further investigated as the next step of the research through a systematic study of samples having small differences of agent penetration depth.

References

1. Sassoni, E., Graziani, G., Franzoni, E. and Scherer, G.W., 2018. Calcium phosphate coatings for marble conservation: Influence of ethanol and isopropanol addition to the precipitation medium on the coating microstructure and performance. *Corrosion Science*, *136*, pp.255-267.

2. Doherty, B., Pamplona, M., Miliani, C., Matteini, M., Sgamellotti, A. and Brunetti, B., 2007. Durability of the artificial calcium oxalate protective on two Florentine monuments. *Journal of Cultural Heritage*, *8*(2), pp.186-192.

3. Calore, N., Botteon, A., Colombo, C., Comunian, A., Possenti, E., Realini, M., Sali, D. and Conti, C., 2018. High Resolution ATR μ-FTIR to map the diffusion of conservation treatments applied to painted plasters. *Vibrational Spectroscopy*, *98*, pp.105-110.

4. Osticioli, I., Botticelli, G., Matteini, P., Siano, S., Pini, R. and Matteini, M., 2017. Micro-Raman analysis on the combined use of ammonium oxalate and ammonium phosphate for the consolidation and protection of carbonate stone artifacts. *Journal of Raman Spectroscopy*, *48*(7), pp.966-971.

5. Possenti, E., Colombo, C., Realini, M., Song, C.L. and Kazarian, S.G., 2021. Time-Resolved ATR–FTIR Spectroscopy and Macro ATR–FTIR Spectroscopic Imaging of Inorganic Treatments for Stone Conservation. *Analytical Chemistry*, *93*(44), pp.14635-14642.

6. Matteini, M., Fratini, F., Rescic, S., Baldan, M., Campana, L. and Cuzman, O.A., 2020. Synergic Use of Ammonium Oxalate and Di-Ammonium Phosphate in the Protection and Consolidation of Carbonate Materials. *International Journal of Conservation Science*, *11*(2), pp.405-424.

7. Celik, S.E., Gulen, J. and Viles, H.A., 2020. Evaluating the effectiveness of DAP as a consolidant on Turkish building stones. *Construction and Building Materials*, *262*, p.120765.

8. Sassoni, E., Ugolotti, G. and Pagani, M., 2020. Nanolime, nanosilica or ammonium phosphate? Laboratory and field study on consolidation of a byzantine marble sarcophagus. *Construction and Building Materials*, *262*, p.120784.

9. Shekofteh, A., Molina, E., Rueda-Quero, L., Arizzi, A. and Cultrone, G., 2019. The efficiency of nanolime and dibasic ammonium phosphate in the consolidation of beige limestone from the Pasargadae World Heritage Site. *Archaeological and Anthropological Sciences*, *11*(9), pp.5065-5080.

10. Franzoni, E., Graziani, G., Sassoni, E., Bacilieri, G., Griffa, M. and Lura, P., 2015. Solvent-based ethyl silicate for stone consolidation: influence of the application technique on penetration depth, efficacy and pore occlusion. *Materials and structures*, *48*(11), pp.3503-3515.

11. Pinto, A.F. and Rodrigues, J.D., 2008. Stone consolidation: The role of treatment procedures. *Journal of Cultural heritage*, *9*(1), pp.38-53.

12. Pinto, A.P.F. and Rodrigues, J.D., 2012. Consolidation of carbonate stones: Influence of treatment procedures on the strengthening action of consolidants. *Journal of cultural heritage*, *13*(2), pp.154-166.

13. Conti, C., Colombo, C., Realini, M., Zerbi, G. and Matousek, P., 2014. Subsurface Raman analysis of thin painted layers. *Applied spectroscopy*, *68*(6), pp.686-691.

14. Mosca, S., Conti, C., Stone, N. and Matousek, P., 2021. Spatially offset Raman spectroscopy. *Nature Reviews Methods Primers*, *1*(1), pp.1-16.

15. Dreyfuss, T., 2020. Artificially induced calcium oxalate on limestone in urban environments–New findings. *Journal of Cultural Heritage*, *42*, pp.56-63.

16. Conti, C., Casati, M., Colombo, C., Realini, M., Brambilla, L. and Zerbi, G., 2014. Phase transformation of

calcium oxalate dihydrate–monohydrate: Effects of relative humidity and new spectroscopic data. *Spectrochimica Acta Part A: Molecular and Biomolecular Spectroscopy*, *128*, pp.413-419.

17. Conti, C., Aliatis, I., Colombo, C., Greco, M., Possenti, E., Realini, M., Castiglioni, C. and Zerbi, G., 2012. µ-Raman mapping to study calcium oxalate historical films. *Journal of Raman Spectroscopy*, *43*(11), pp.1604-1611.

18. Matteini, M., Sescic, S. and Fratini, F., 2007. Carbonatic Lithotypes Passivated with the'Ammonium Oxalate Treatment': Colorimetric and Morphological Study of Treated Surfaces. *Carbonatic Lithotypes Passivated with the'Ammonium Oxalate Treatment'*, pp.1000-1013.

19. Matteini, M., Colombo, C., Botticelli, G., Casati, M., Conti, C., Negrotti, R., Possenti, E. and Realini, M., 2013. Ammonium phosphates to consolidate carbonatic stone materials: An inorganic-mineral treatment greatly promising. Proceedings of Conference *Built Heritage 2013 - Monitoring Conservation and Management Milan* - Italy, 18-20 November 2013

20. Mudronja, D., Vanmeert, F., Fazinic, S., Janssens, K., Tibljas, D. and Desnica, V., 2021. Protection of Stone Monuments Using a Brushing Treatment with Ammonium Oxalate. *Coatings*, *11*(4), p.379.

21. Matteini, M., 2008. Inorganic treatments for the consolidation and protection of stone artefacts. *Conservation science in cultural heritage*, *8*, pp.13-27.

22. Conti, C., Colombo, C., Matteini, M., Realini, M. and Zerbi, G., 2010. Micro-Raman mapping on polished cross sections: a tool to define the penetration depth of conservation treatment on cultural heritage. *Journal of Raman Spectroscopy*, *41*(10), pp.1254-1260.

23. Conti, C., Colombo, C., Dellasega, D., Matteini, M., Realini, M. and Zerbi, G., 2011. Ammonium oxalate treatment: evaluation by µ-Raman mapping of the penetration depth in different plasters. *Journal of cultural heritage*, *12*(4), pp.372-379.

24. Conti, C., Colombo, C., Festa, G., Hovind, J., Cippo, E.P., Possenti, E. and Realini, M., 2016. Investigation of ammonium oxalate diffusion in carbonatic substrates by neutron tomography. *Journal of Cultural Heritage*, *19*, pp.463-466.

25. Realini, M., Colombo, C., Conti, C., Grazzi, F., Perelli Cippo, E. and Hovind, J., 2017. Development of neutron imaging quantitative data treatment to assess conservation products in cultural heritage. *Analytical and bioanalytical chemistry*, *409*(26), pp.6133-6139.

26. Conti, C., Realini, M., Colombo, C. and Matousek, P., 2015. Comparison of key modalities of micro-scale spatially offset Raman spectroscopy. *Analyst*, *140*(24), pp.8127-8133.

27. Botteon, A., Yiming, J., Prati, S., Sciutto, G., Realini, M., Colombo, C., Castiglioni, C., Matousek, P. and Conti, C., 2020. Non-invasive characterisation of molecular diffusion of agent into turbid matrix using micro-SORS. *Talanta*, *218*, p.121078.

28. Jia, Y., Sciutto, G., Botteon, A., Conti, C., Focarete, M.L., Gualandi, C., Samorì, C., Prati, S. and Mazzeo, R., 2021. Deep eutectic solvent and agar: a new green gel to remove proteinaceous-based varnishes from paintings. *Journal of Cultural Heritage*, *51*, pp.138-144.

29. Botteon, A., Realini, M., Colombo, C., Conti, C., Matousek, P. and Castiglioni, C., 2021. Micro-SORS, diffusion processes and heritage science: a non-destructive and systematic investigation. *The European Physical Journal Plus*, *136*(8), pp.1-12.